

Chapter 4

ELECTRON RECONSTRUCTION AND IDENTIFICATION AT ATLAS

Not all chapters are about improving selections, only one, say reconstruction and identification

Type

Rephrase, it's not the chapter that measures

Rephrase, it's not the chapter that measures
Replace simply by introduces

Define signal electron, i.e. prompt isolated electron from the decay of a W, Z or H boson or a BSM particle.

This is as vague as it can be, it contains almost negative information. Say that it applies criteria on tracking and calorimeter variables to select signal electrons

With the

These sentences, which discuss the fact that electrons radiate, are good by themselves but they have no link to the bullets that describe electron reconstruction but without addressing photon recovery. Not sure what was the intent but need significant rephrasing

The central theme of this thesis is the improvement of the selection of signal electrons in SUSY searches. In particular, Chapter 5 deals with the estimation of electron charge mis-identification, Chapter 6 discusses a supersymmetry search that involves leptons (electrons or muons) in the final state, and Chapter 7 measures the identification efficiencies for in-jet electrons¹. This chapter presents a more extended discussion of electron reconstruction and identification at ATLAS [37].

At ATLAS, a signal electron that has been selected passes through two major steps, reconstruction and identification. Electron reconstruction, discussed in Section 4.1, is the selection, using information from the inner detector and the electromagnetic calorimeter, of a set of objects which are called electron candidates. Electron identification, on the other hand, refers to the selection from a pool of electron candidates; it is discussed in Section 4.2.

Figure 4.1 [37] shows the hypothetical path of an electron, in red trajectory, through the ATLAS detector. The electron emerges near the collision point, passes the tracking system (made up of the pixel detectors, the silicon-strip detectors, and the TRT) before entering the electromagnetic calorimeter. Also shown in the figure is the path of a photon, in dashed trajectory, produced by the interaction of the electron with the material in the tracking system.

4.1 Electron Reconstruction

At ATLAS, we expect most electrons passing through the detector to interact with the material of the latter and lose a significant amount of energy through bremsstrahlung. These interactions, which may happen along the path of the electrons, typically cause radiated photons and consequently electron-positron pairs, all of which tend to collimate. Thus, electron reconstruction at ATLAS consists of three fundamental components:

¹These refer to electrons that are found within $\Delta R = 0.4$ of high p_T jets.

824 Chapter 4

825 ELECTRON 826 RECONSTRUCTION AND 827 IDENTIFICATION AT ATLAS

828 The central theme of this thesis is the improvement of the reconstruction and identifi-
829 cation of signal electrons in SUSY searches. In particular, Chapter 5 deals with the
830 estimation of electron charge mis-identification, Chapter 6 discusses a supersymme-
831 try search that involves leptons (electrons or muons) in the final state where work on
832 improving the lepton selection will be presented, and Chapter 7 presents a measure-
833 ment of the identification efficiencies for in-jet electrons¹. This chapter introduces
834 electron reconstruction and identification at ATLAS [38].

835 At ATLAS, a signal (prompt) electron² that has been selected passes through two
836 major steps, reconstruction and identification. Electron reconstruction, discussed
837 in Section 4.1, is the selection, using information from the inner detector and the
838 electromagnetic calorimeter, of a set of objects which are called electron candidates.
839 Electron identification, on the other hand, applies criteria on tracking and calorimeter
840 variables to select signal electrons; it is discussed in Section 4.2.

841 Figure 4.1 [38] shows the hypothetical path of an electron, in the red trajectory,
842 through the ATLAS detector. The electron emerges near the collision point, passes
843 the tracking system (made up of the pixel detectors, the silicon-strip detectors, and
844 the TRT) before entering the electromagnetic calorimeter. Also shown in the figure
845 is the path of a photon, in dashed trajectory, produced by the interaction of the
846 electron with the material in the tracking system.

847 4.1 Electron Reconstruction

848 At ATLAS, we expect most electrons passing through the detector to interact with
849 the material of the latter and lose a significant amount of energy through bremsstrahlung.
850 Such a process could take place at different points along the path of an electron and
851 typically causes radiated photons and consequently electron-positron pairs, all of

¹These refer to electrons that are found within $\Delta R = 0.4$ of high p_T jets.

²This is an electron that originates from the prompt decays of particles such as W , Z , and other beyond the Standard Model particles.

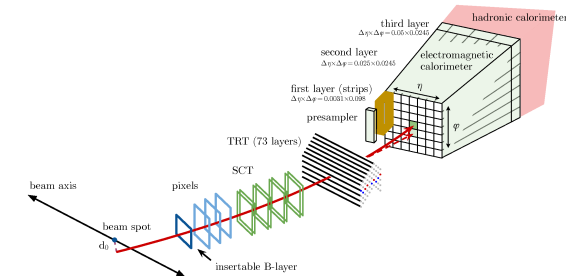
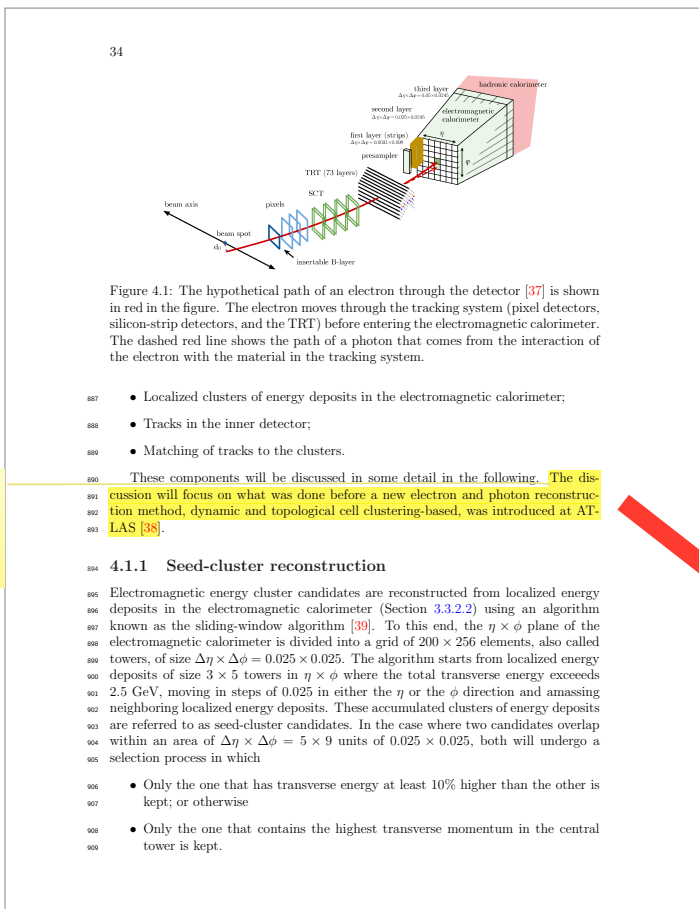


Figure 4.1: The hypothetical path of an electron through the detector [38] is shown in red in the figure. The electron moves through the tracking system (pixel detectors, silicon-strip detectors, and the TRT) before entering the electromagnetic calorimeter. The dashed red line shows the path of a photon that comes from the interaction of the electron with the material in the tracking system.

852 which tend to collimate and are normally reconstructed as part of the same elec-
 853 tron magnetic cluster. These interactions, initiated by the primary electron, could
 854 generate multiple tracks in the inner detector or impact the electromagnetic shower
 855 in the electromagnetic calorimeter.

856 Electron reconstruction at ATLAS consists of three fundamental components that
 857 characterize the signature of electrons:

- 858 • Localized clusters of energy deposits in the electromagnetic calorimeter;
- 859 • Tracks in the inner detector;
- 860 • Matching of tracks to the clusters.

861 These components will be discussed in some detail in the following. As this
 862 thesis is based on 2015-2016 data (analyzed by release 20 of the ATLAS software), the
 863 discussion focuses on the methods used prior to the introduction of a new electron and
 864 photon reconstruction method, dynamic and topological cell clustering-based [39] (in
 865 release 21 of the ATLAS software).

866 **4.1.1 Seed-cluster reconstruction**

867 Electromagnetic energy cluster candidates are reconstructed from localized energy
 868 deposits in the electromagnetic calorimeter (Section 3.3.2.2) using an algorithm
 869 known as the sliding-window algorithm [40]. To this end, the $\eta \times \phi$ plane of the
 870 electromagnetic calorimeter is divided into a grid of 200×256 elements, also called
 871 towers, of size $\Delta\eta \times \Delta\phi = 0.025 \times 0.025$. The algorithm starts from localized energy
 872 deposits of size 3×5 towers in $\eta \times \phi$ where the total transverse energy exceeds
 873 2.5 GeV, moving in steps of 0.025 in either the η or the ϕ direction and amassing
 874 neighboring localized energy deposits. These accumulated clusters of energy deposits

It's the cluster reco efficiency right? Specify.
Also clarify the caption of the figure. Relative
to reco cluster is confusing because it's
suggest the denominator is reco cluster, use
a less ambiguous phrasing

⁹¹⁰ The reconstruction efficiency is found to depend on η and on the transverse
⁹¹¹ energy. Figure 4.2 shows the dependency on E_T . The efficiency ranges from 96% at
⁹¹² $E_T = 7$ GeV to more than 99% above $E_T = 15$ GeV.

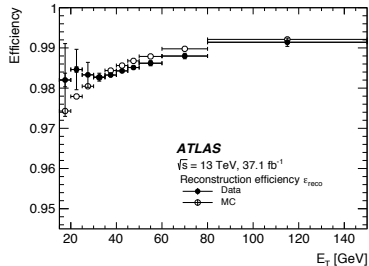


Figure 4.2: The reconstruction efficiency relative to reconstructed clusters as a function of E_T for $Z \rightarrow ee$ events.

4.1.2 Track reconstruction

The interactions of charged particles with the inner detector material created hits [40] in the latter. In track reconstruction, these hits are assembled into clusters in the pixel and SCT detectors, from which three-dimensional measurements called space-points are built. In the silicon-detector layers, sets of three space-points are used to form track seeds. Then a pattern-recognition algorithm proceeds to build track candidates, in which energy loss of a particle due to its interactions with the detector material is modelled assuming the particle is a pion. A modified pattern-recognition will be used in the case where a track seed having $p_T > 1$ GeV cannot be extended to a full track of at least seven hits per track candidate and the associated electromagnetic calorimeter cluster satisfies shower width and depth requirements. The modified algorithm allows up to 30% energy loss for bremsstrahlung at each intersection of the track with the detector material.

Track candidates with $p_T > 400$ MeV are fit using the ATLAS Global χ^2 Track Fitter [41], taking into account which pattern-recognition algorithm was used. Ambiguities arising from track candidates sharing hits are also resolved in this step.

Figure 4.3 shows that the reconstruction efficiency ranges from 80% at $E_T = 1$ GeV to more than 98% above $E_T = 10$ GeV.

An additional fit, using the Gaussian-sum filter (GSF) [42] method to better model energy loss of the particle, is applied on tracks having at least four silicon hits and that are loosely matched to electromagnetic clusters. The method takes into

That the electron track reconstruction efficiency. Or you mean the total? Talk about the total something like that is what you were just talking about. Clarify the caption of the figure, it's not only the total but also the electron track reconstruction efficiency. Also don't quote efficiency numbers below Pt of 5 GeV, atlas never use electrons below 5 GeV

⁸⁷⁵ are referred to as seed-cluster candidates. In the case where two candidates overlap
⁸⁷⁶ within an area of $\Delta\eta \times \Delta\phi = 5 \times 9$ units of 0.025×0.025 , both will undergo a
⁸⁷⁷ selection process in which

- ⁸⁷⁸ • Only the one that has transverse energy at least 10% higher than the other is kept; or otherwise
- ⁸⁸⁰ • Only the one that contains the highest transverse momentum in the central tower is kept.

⁸⁸² The reconstruction efficiency of this seed-cluster algorithm is found to depend on η and on the transverse energy. Figure 4.2 shows the dependency on E_T . The efficiency ranges from 96% at $E_T = 7$ GeV to more than 99% above $E_T = 15$ GeV.

4.1.2 Track reconstruction

⁸⁸⁶ The interactions of charged particles with the inner detector material created hits [41]
⁸⁸⁷ in the latter. In track reconstruction, these hits are assembled into clusters in the
⁸⁸⁸ pixel and SCT detectors, from which three-dimensional measurements called
⁸⁸⁹ space-points are built. In the silicon-detector layers, sets of three space-points are used
⁸⁹⁰ to form track seeds. Then a pattern-recognition algorithm proceeds to build track
⁸⁹¹ candidates, in which energy loss of a particle due to its interactions with the detector
⁸⁹² material is modelled assuming the particle is a pion. A modified pattern-recognition
⁸⁹³ will be used in the case where a track seed having $p_T > 1$ GeV cannot be extended to a
⁸⁹⁴ full track of at least seven hits per track candidate and the associated electromagnetic
⁸⁹⁵ calorimeter cluster satisfies shower width and depth requirements. The modified
⁸⁹⁶ algorithm allows up to 30% energy loss for bremsstrahlung at each intersection of
⁸⁹⁷ the track with the detector material.

⁸⁹⁸ Track candidates with $p_T > 400$ MeV are fit using the ATLAS Global χ^2 Track
⁸⁹⁹ Fitter [42], taking into account which pattern-recognition algorithm was used. Am-
⁹⁰⁰ biguities arising from track candidates sharing hits are also resolved in this step.
⁹⁰¹ Figure 4.2 shows that the reconstruction efficiency of the track-fitting step reaches
⁹⁰² more than 98% above $E_T = 10$ GeV.

⁹⁰³ An additional fit, using the Gaussian-sum filter (GSF) [43] method to better
⁹⁰⁴ model energy loss of the particle, is applied on tracks having at least four silicon hits
⁹⁰⁵ and that are loosely matched to electromagnetic clusters. The method takes into
⁹⁰⁶ account non-linear effects related to bremsstrahlung and models experimental noise
⁹⁰⁷ by a sum of Gaussian functions.

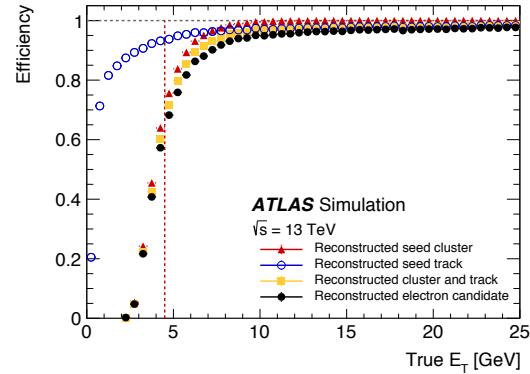
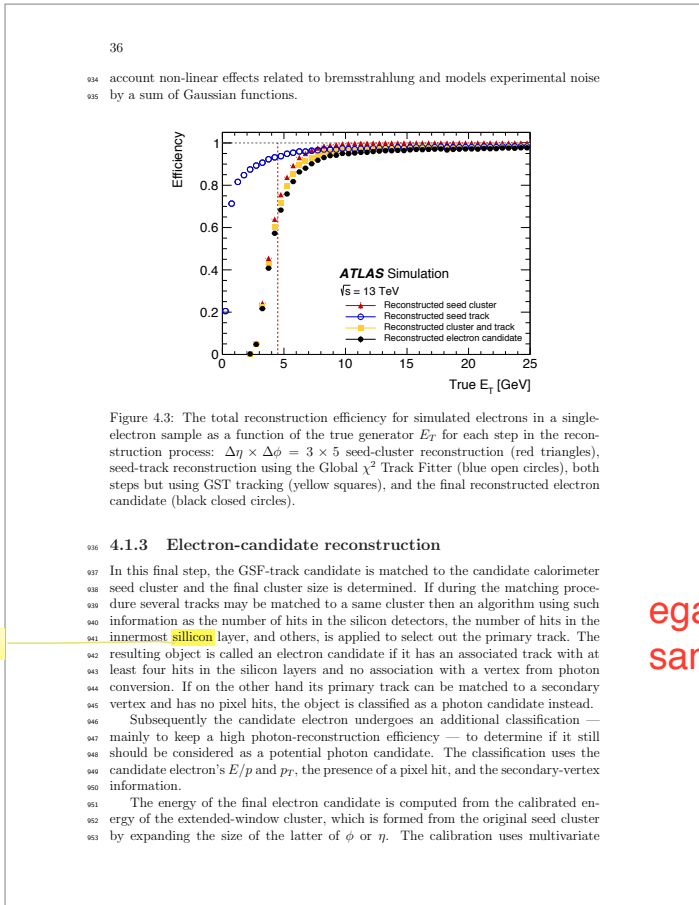


Figure 4.2: The efficiencies for simulated electrons in a single-electron sample as a function of the true generator E_T for each step in the reconstruction process, as well as the total efficiency: $\Delta\eta \times \Delta\phi = 3 \times 5$ seed-cluster reconstruction (red triangles), seed-track reconstruction using the Global χ^2 Track Fitter (blue open circles), both steps but using GST tracking (yellow squares), and the final reconstructed electron candidate (black closed circles).

4.1.3 Electron-candidate reconstruction

In this final step, the GSF-track candidate is matched to the candidate calorimeter seed cluster and the final cluster size is determined. If during the matching procedure several tracks may be matched to a same cluster then an algorithm using such information as the number of hits in the silicon detectors, the number of hits in the innermost silicon layer, and others, is applied to select out the primary track. The resulting object is called an electron candidate if it has an associated track with at least four hits in the silicon layers and no association with a vertex from photon conversion. If on the other hand its primary track can be matched to a secondary vertex and has no pixel hits, the object is classified as a photon candidate instead. Subsequently the candidate electron undergoes an additional classification — mainly to keep a high photon-reconstruction efficiency — to determine if it still should be considered as a potential photon candidate. The classification uses the candidate electron's E/p and p_T , the presence of a pixel hit, and the secondary-vertex information.

The energy of the final electron candidate is computed from the calibrated energy of the extended-window cluster, which is formed from the original seed cluster by expanding the size of the latter of ϕ or η . The calibration uses multivariate techniques [45, 46].

Figure 4.2 and 4.3 show the total reconstruction efficiency as a function of E_T and as a function of η in bins of E_T , respectively, from $Z \rightarrow e^+e^-$ events. This efficiency

show the total reconstruction... Also explain in one sentence how this efficiency is measured. Not obvious a priori, I'm not sure myself what is the denominator of that measurement.

Quote an approximate number

Type
Tune

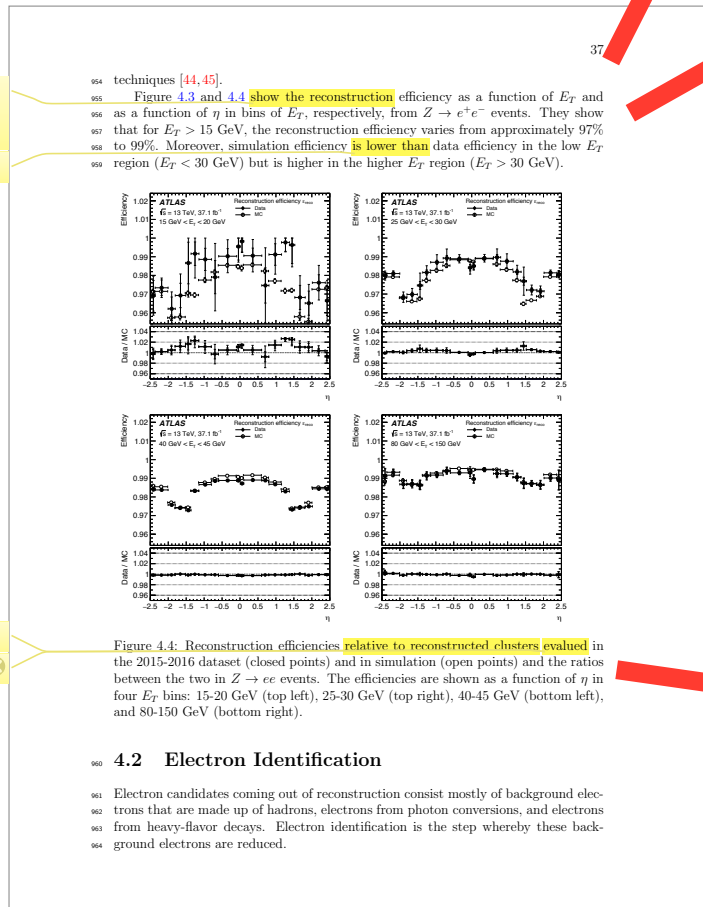


Figure 4.4: Reconstruction efficiencies relative to reconstructed clusters evaluated in the 2015-2016 dataset (closed points) and in simulation (open points) and the ratios between the two in $Z \rightarrow ee$ events. The efficiencies are shown as a function of η in four E_T bins: 15-20 GeV (top left), 25-30 GeV (top right), 40-45 GeV (bottom left), and 80-150 GeV (bottom right).

4.2 Electron Identification

Electron candidates coming out of reconstruction consist mostly of background electrons that are made up of hadrons, electrons from photon conversions, and electrons from heavy-flavor decays. Electron identification is the step whereby these background electrons are reduced.

is defined as the ratio of the number of reconstructed electron candidates and the number of electromagnetic-cluster candidates. For $E_T > 15$ GeV, the reconstruction efficiency varies from approximately 97% to 99%. Moreover, simulation efficiency is lower than data efficiency (up to $\sim 25\%$) in the low E_T region ($E_T < 30$ GeV) but is higher (up to a few percents) in the higher E_T region ($E_T > 30$ GeV).

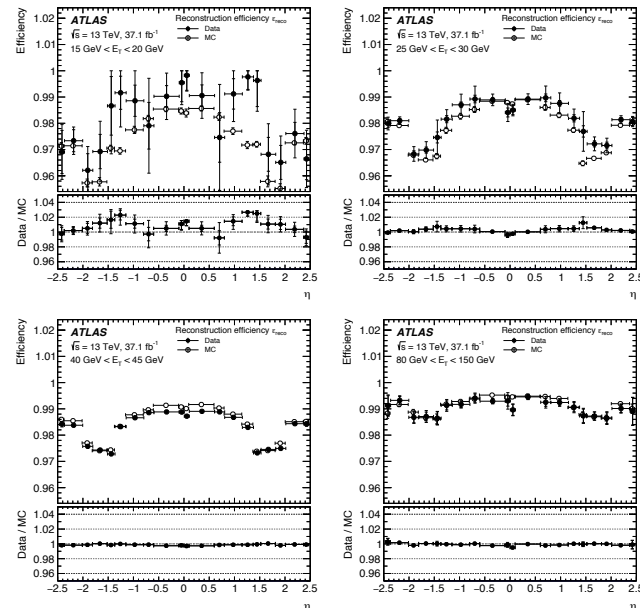


Figure 4.3: The total reconstruction efficiencies, defined as the ratio of the number of reconstructed electron candidates and the number of electromagnetic-cluster candidates, evaluated in the 2015-2016 dataset (closed points) and in simulation (open points). The efficiencies are shown as a function of η in four E_T bins: 15-20 GeV (top left), 25-30 GeV (top right), 40-45 GeV (bottom left), and 80-150 GeV (bottom right).

4.2 Electron Identification

Electron candidates coming out of reconstruction consist mostly of background electrons that are made up of hadrons, electrons from photon conversions, and electrons from heavy-flavor decays. Electron identification is the step whereby these background electrons are reduced.

4.2.1 Likelihood Identification

Prompt electrons² that enter the central region ($|\eta| < 2.47$) are selected using a method called the likelihood identification. In this method, the differences in shower shapes, in track conditions, penetration depth, and others between prompt electrons and background electrons are analyzed in detail. Specifically, the following quantities [37], which are classified into seven types, are used:

I thought
this way could
be more efficient

Nowhere is the physics explaining the differences between the signatures of signal and background electrons is explained. See specific suggestion below

As mentioned before, move this definition earlier, and apply it to signal electrons. In the method, differences between signal and background electron candidates in terms of shower shapes,....

Next to the title of each category below you could explain in 1-2 sentences the physics of why these variables are useful. E.g here it's because hadronic showers are longer than EM showers

Same reason as above

EM showers are narrower than HAD showers

Explanation to be found depending on the meaning of each variable. If the definition of the variables is too complicated, provide a qualitative explanation only focusing on the physics

These variables are not intuitive and undefined

defined up

4.2.1 Likelihood Identification

Prompt electrons² that enter the central region ($|\eta| < 2.47$) are selected using a method called the likelihood identification. In this method, the differences in shower shapes, in track conditions, penetration depth, and others between prompt electrons and background electrons are analyzed in detail. Specifically, the following quantities [37], which are classified into seven types, are used:

- Hadronic leakage
 - $R_{\text{had}1}$: Ratio of the transverse momentum in the first layer of the Hadronic Calorimeter to that of the Electromagnetic Calorimeter.
 - $R_{\text{had}2}$: Ratio of the transverse momentum in the Hadronic Calorimeter to that of the Electromagnetic Calorimeter cluster (used in range $0.8 < |\eta| < 1.37$).
- Third layer of EM calorimeter
 - f_3 : Ratio of the energy in the third layer to the total energy in the Electromagnetic Calorimeter (used only for $E_T < 80$ GeV).
- Second layer of EM calorimeter
 - ω_{η^2} : Lateral shower width.
 - R_ϕ : Ratio of the energy in 3×3 cells over the energy in 3×7 cells centered at the electron cluster position.
 - R_η : Ratio of the energy in 3×7 cells over the energy in 7×7 cells centered at the electron cluster position.
- First layer of EM calorimeter
 - ω_{stot}
 - E_{ratio}
 - f_1
- Track conditions
 - n_{Blayer} : the number of hits in the innermost pixel layer.
 - n_{Pixel} : the number of hits in the Pixel detector.
 - n_{Si} : the total number of hits in the pixel and SCT detectors.
 - d_0
 - $|d_0/\sigma(d_0)|$
 - $\Delta p/p$
- TRT

²These refer to electrons that originate from the prompt decays of particles such as W , Z , and other beyond the Standard Model particles.



- Hadronic leakage.

- $R_{\text{had}1}$: Ratio of the transverse momentum in the first layer of the Hadronic Calorimeter to that of the Electromagnetic Calorimeter.
- $R_{\text{had}2}$: Ratio of the transverse momentum in the Hadronic Calorimeter to that of the Electromagnetic Calorimeter cluster (used in range $0.8 < |\eta| < 1.37$).

- Third layer of EM calorimeter

- f_3 : Ratio of the energy in the third layer to the total energy in the Electromagnetic Calorimeter (used only for $E_T < 80$ GeV).

- Second layer of EM calorimeter

- ω_{η^2} : Lateral shower width.
- R_ϕ : Ratio of the energy in 3×3 cells over the energy in 3×7 cells centered at the electron cluster position.
- R_η : Ratio of the energy in 3×7 cells over the energy in 7×7 cells centered at the electron cluster position.

- First layer of EM calorimeter

- ω_{stot} : Shower width.
- E_{ratio} : Ratio of the energy difference between the maximum energy deposit and the energy deposit in a secondary maximum in the cluster to the sum of these energies.
- f_1 : Ratio of the energy in the first layer to the total energy in the EM calorimeter.

- Track conditions

- n_{Blayer} : The number of hits in the innermost pixel layer.
- n_{Pixel} : The number of hits in the Pixel detector.
- n_{Si} : The total number of hits in the pixel and SCT detectors.
- d_0 : Transverse impact parameter relative to the beam-line.

Undefined

998 – eProbabilityHT

999 • Track-cluster matching

1000 – $\Delta\eta$: $\Delta\eta$ between the cluster position in the first layer and the extrapolated track

1001 – $\Delta\phi_{\text{res}}$

1002 – E/p : ratio of the cluster energy to the track momentum (for $E_T > 150$ GeV)

1003 These are used as inputs to two likelihood functions, one for signal electrons and one for background electrons, which take the forms

1004

$$L_S(\mathbf{x}) = \prod_{i=1}^n P_{S,i}(x_i), \quad L_B(\mathbf{x}) = \prod_{i=1}^n P_{B,i}(x_i)$$

1005 respectively. Here \mathbf{x} is a vector of entries x_i which are the inputs that correspond to the quantities listed above, each of which has a signal probability distribution function (pdf) and a background pdf. $P_{S,i}(x_i)$ is the value of the signal pdf of the quantity i at the value x_i , and likewise $P_{B,i}(x_i)$ is the value of the background pdf. The pdfs are derived using simulation samples, with corrections applied when discrepancies with the corresponding data are found. The correlations between the inputs are neglected.

1006 Then, from each electron candidate discriminant value d_L is computed according to the formula

1007

$$d_L = \frac{L_S}{L_S + L_B}$$

1008 This discriminant is actually transformed into

1009

$$d'_L = -\tau^{-1} \ln(d_L^{-1} - 1) \quad (4.1)$$

1010 which then serves as a quantity to assess if an electron candidate should be considered a prompt electron. The parameter τ is set to 15 [43]. Figure 4.5 shows a comparison of d_L and d'_L for prompt electrons from Z -boson decays and for background, illustrating the effective separation between the two.

1011

4.2.2 Operating Points

1012 In general, background rejection and identification efficiency are inversely related i.e. the higher is one, the lower is the other, and vice versa. In order to cover various signal efficiencies and background rejection factors as needed by physics analyses, ATLAS has defined four so-called identification operating points. They are, in order of increasing background rejection power, VeryLoose, Loose, Medium, and Tight. All operating points have fixed requirements on tracking criteria:

1013

- Loose, Medium, and Tight: at least two hits in the Pixel detector and a total of seven hits in the pixel and silicon strip detectors combined. To reduce

Figure 4.5 only shows d'_L ; rephrase

Remove "in general", this statement is always true

39

976 – $|d_0/\sigma(d_0)|$: Significance of transverse impact parameter defined as the ratio of d_0 to its uncertainty.

977 – $\Delta p/p$: Momentum lost by the track between the perigee and the last measurement point divided by the momentum at perigee.

980 • TRT

981 – eProbabilityHT: Likelihood probability based on transition radition in the TRT.

983 • Track-cluster matching

984 – $\Delta\eta$: $\Delta\eta$ between the cluster position in the first layer and the extrapolated track

985 – $\Delta\phi_{\text{res}}$: $\Delta\phi$ between the cluster position in the second layer of the EM calorimeter and the momentum-rescaled track, extrapolated from the perigee, times the charge q

986 – E/p : ratio of the cluster energy to the track momentum (for $E_T > 150$ GeV)

991 These are used as inputs to two likelihood functions, one for signal electrons and 992 one for background electrons, which take the forms

$$L_S(\mathbf{x}) = \prod_{i=1}^n P_{S,i}(x_i), \quad L_B(\mathbf{x}) = \prod_{i=1}^n P_{B,i}(x_i)$$

993 respectively. Here \mathbf{x} is a vector of entries x_i which are the inputs that correspond 994 to the quantities listed above, each of which has a signal probability distribution 995 function (pdf) and a background pdf. $P_{S,i}(x_i)$ is the value of the signal pdf of 996 the quantity i at the value x_i , and likewise $P_{B,i}(x_i)$ is the value of the background 997 pdf. The pdfs are derived using simulation samples, with corrections applied when 998 discrepancies with the corresponding data are found. The correlations between the 999 inputs are neglected.

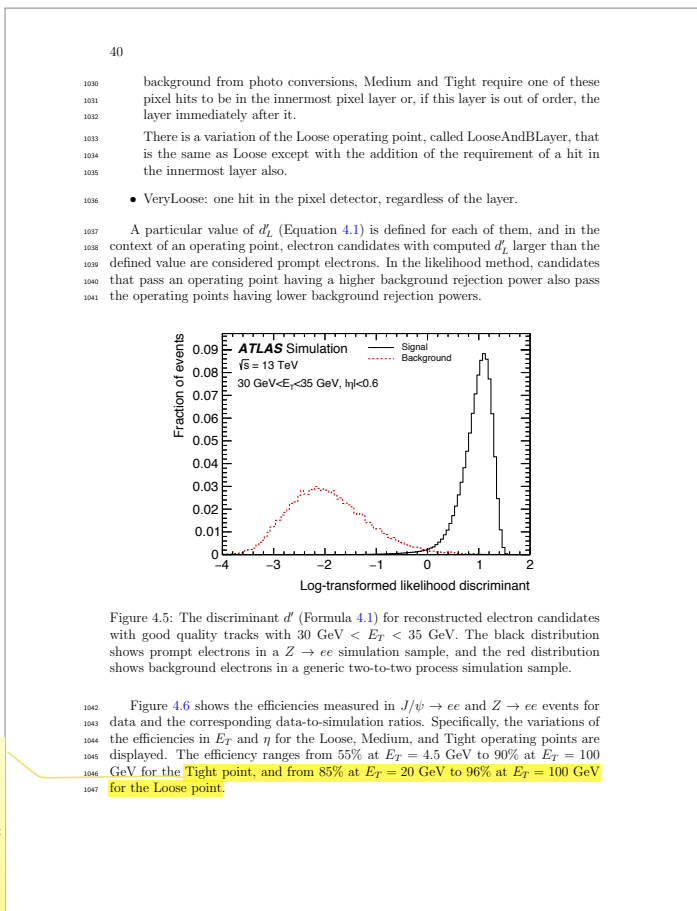
1000 Then, from each electron candidate discriminant value d_L is computed according 1001 to the formula

$$d_L = \frac{L_S}{L_S + L_B}$$

1002 This discriminant is actually transformed into

$$d'_L = -\tau^{-1} \ln(d_L^{-1} - 1) \quad (4.1)$$

1003 which then serves as a quantity to assess if an electron candidate should be 1004 considered a prompt electron. The parameter τ is set to 15 [44]. Figure 4.4 shows 1005 the transformed discriminant d'_L for prompt electrons from Z -boson decays and for 1006 background, illustrating the effective separation between the two.



42

4.2.2 Operating Points

Background rejection and identification efficiency are inversely related i.e. the higher is one, the lower is the other, and vice versa. In order to cover various signal efficiencies and background rejection factors as needed by physics analyses, ATLAS has defined four so-called identification operating points. They are, in order of increasing background rejection power, VeryLoose, Loose, Medium, and Tight. All operating points have fixed requirements on tracking criteria:

- Loose, Medium, and Tight: at least two hits in the Pixel detector and a total of seven hits in the pixel and silicon strip detectors combined. To reduce background from photo conversions, Medium and Tight require one of these pixel hits to be in the innermost pixel layer or, if this layer is out of order, the layer immediately after it.

There is a variation of the Loose operating point, called LooseAndBLayer, that is the same as Loose except with the addition of the requirement of a hit in the innermost layer also.

- VeryLoose: one hit in the pixel detector, regardless of the layer.

A particular value of d'_L (Equation 4.1) is defined for each of them, and in the context of an operating point, electron candidates with computed d'_L larger than the defined value are considered prompt electrons. In the likelihood method, candidates that pass an operating point having a higher background rejection power also pass the operating points having lower background rejection powers.

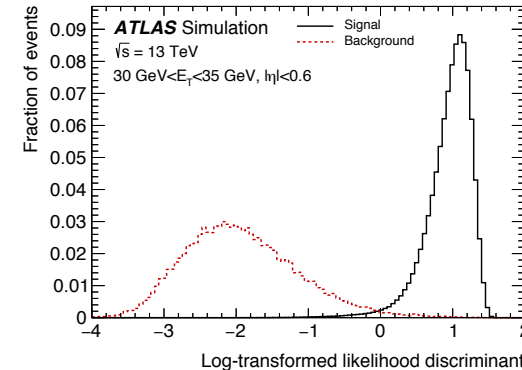


Figure 4.4: The discriminant d' (Formula 4.1) for reconstructed electron candidates with good quality tracks with $30 \text{ GeV} < E_T < 35 \text{ GeV}$. The black distribution shows prompt electrons in a $Z \rightarrow ee$ simulation sample, and the red distribution shows background electrons in a generic two-to-two process simulation sample.

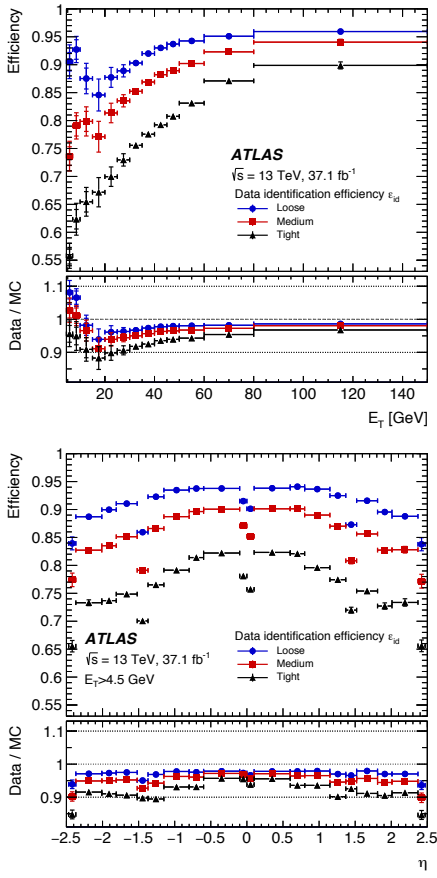


Figure 4.6: The likelihood identification efficiencies as functions of E_T and η in $Z \rightarrow ee$ events for Loose, Medium, and Tight (shown in blue, red, and black respectively). The data efficiencies are obtained by applying data-to-simulation efficiency ratios measured in $J/\psi \rightarrow ee$ and $Z \rightarrow ee$ events to $Z \rightarrow ee$ simulation.



Figure 4.5 shows the efficiencies measured in $J/\psi \rightarrow ee$ and $Z \rightarrow ee$ events for data and the corresponding data-to-simulation ratios. Specifically, the variations of the efficiencies in E_T and η for the Loose, Medium, and Tight operating points are displayed. The efficiency ranges from 55% at $E_T = 4.5$ GeV to 90% at $E_T = 100$ GeV for the Tight point, and from 85% at $E_T = 20$ GeV to 96% at $E_T = 100$ GeV for the Loose point. On the other hand, the efficiency decreases as we move to higher $|\eta|$, the decreases could be as big as 10%. The lower efficiencies of the Medium and Tight operating points result in an increased rejection of background. In the E_T range of 4 – 50 GeV, the rejection factors for misidentified electrons from multijet production increase by factors of ~ 2.5 for the Medium point and ~ 5 for the Tight point compared to the Loose point [38].

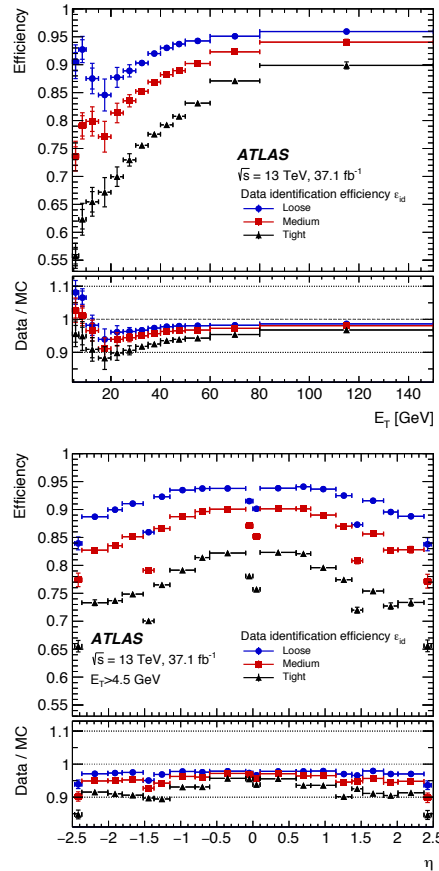


Figure 4.6: The likelihood identification efficiencies as functions of E_T and η in $Z \rightarrow ee$ events for Loose, Medium, and Tight (shown in blue, red, and black respectively). The data efficiencies are obtained by applying data-to-simulation efficiency ratios measured in $J/\psi \rightarrow ee$ and $Z \rightarrow ee$ events to $Z \rightarrow ee$ simulation.

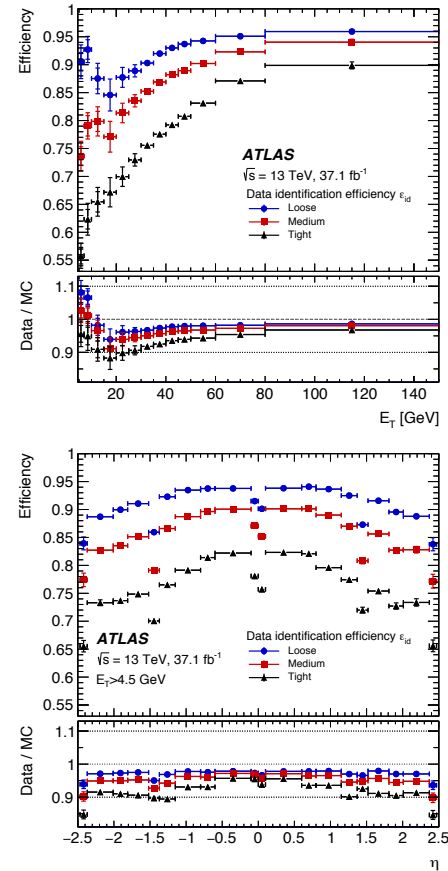


Figure 4.5: The likelihood identification efficiencies as functions of E_T and η in $Z \rightarrow ee$ events for Loose, Medium, and Tight (shown in blue, red, and black respectively). The data efficiencies are obtained by applying data-to-simulation efficiency ratios measured in $J/\psi \rightarrow ee$ and $Z \rightarrow ee$ events to $Z \rightarrow ee$ simulation.